This article has been accepted for publication in a future issue of this journal, but has not been fully edited. Content may change prior to final publication. Citation information: DOI 10.1109/TAP.2021.3111280, IEEE Transactions on Antennas and Propagation

Single-Fed Triple-Mode Wideband Circularly Polarized Microstrip Antennas Using Characteristic Mode Analysis

Jianping Zeng, *Student Member, IEEE*, Xiuye Liang, Lianxing He, Fang Guan, Feng Han Lin, *Senior Member, IEEE*, and Jian Zi

***Abstract*—A method of triple-mode operation by capacitive slot loading is proposed for bandwidth enhancement of single-fed circularly polarized (CP) patch antennas. Instead of using even-numbered linearly polarized (LP) modes with quadrature phase, three orthogonal LP modes are used to CP bandwidth enhancement, where the middle mode is shared by two cross-polarized modes with the same polarization. The advantages include reduced constraints, lower complexity and higher degree of freedom for antenna design. Guided by the method, a U-slot antenna and an E-shaped antenna are proposed and designed with characteristic mode analysis (CMA). Both antennas work with a TM_{10}-like mode and a TM_{01}-like mode. Differently, the U-slot antenna works with an additional slot mode and the E-shaped antenna works with an additional TM_{11}-like mode. The operating modes are manipulated by the slot loadings for creating phase difference. As a result, wideband CP radiation is achieved with single feeding. CMA-based empirical formulas are derived for fast design. The proposed method and antennas are experimentally validated. Both antennas measure a bandwidth exceeding 21% for 10-dB return loss and 3-dB axial-ratio (AR), a significant improvement compared with conventional corner-truncated U-slot patch antennas of similar thickness or volume.**

***Index Terms*—Axial-ratio (AR), characteristic mode analysis (CMA), circularly polarized (CP), E-shaped antenna, triple-mode resonance, U-slot antenna, wideband.**

I. Introduction

CIRCULARLY polarized (CP) antennas are demanded in wireless systems for reduced multi-path interferences and flexible orientations between transmitting and receiving antennas [1]–[2]. Microstrip patch antenna is an attractive candidate due to its low profile, low cost and ease of fabrication [3]–[5]. However, due to the inherently narrow bandwidth of microstrip antennas, it is challenging to design single-fed and wideband CP microstrip patch antenna without increasing the antenna volume significantly [6]–[8].

Wideband CP microstrip patch antennas can be achieved with multi-fed or single-fed techniques [1]. Comparing with the multi-fed technique which needs additional complex feeding network [9], [10], single-fed antennas are attractive for their simplicity in phased array applications. Normally, for single-fed CP microstrip antennas, the axial-ratio (AR) bandwidth can be enhanced by lowering the Q-factor of two orthogonal linearly polarized (LP) modes by using thick substrates of low-permittivity [11]–[14]. Furthermore, approaches of U-slot patch [15]–[21], E-shaped patch [22]–[25], and L-probe [26]–[29] are also effectively for improving the impedance matching. However, most of the aforementioned approaches are less effective for AR bandwidth enhancement than for impedance bandwidth. CP bandwidth is still limited. For example, the maximum CP bandwidth reported in reference [27] is only 11.8%, which is still not satisfied, but the thickness of the patch antenna has been increased to $0.221\lambda_0$. In short, this method tends to increase the antenna volume significantly.

Alternatively, multiple pairs of orthogonal modes can be leveraged for improving the AR bandwidth by parasitic loadings, such as stacked layers and coplanar parasitic elements [30]–[34]. However, when it comes to multi-mode CP radiation, the loading method usually lacks of clear design guideline to address the phase difference between excited modes to form multi-mode CP radiation. In theory, a CP mode can be decomposed into two LP modes of quadrature phase difference. Straightforwardly, two CP modes need four LP modes. As a result, multiple CP modes lead to typically an even number of LP modes. This stresses certain symmetries for the patch geometry hence limiting the design freedom. Also, the mode theory of multi-mode CP antennas becomes more complicated. 5% of CP bandwidth has been realized by creative use of triple modes in [35], where the use of a higher-order $TM_{3/2,0}$ mode may hinder further bandwidth improvement of CP antennas of low sidelobes. The adopted method is by loading metallic vias, corresponding to *inductive loading* of patch antennas.

Characteristic mode analysis (CMA) has recently regained its applications in the analysis and design of antennas, though proposed in early 1960s [36]–[38]. The revealed physical understanding helps with the improvement of antenna performances in multiple contexts, such as bandwidth enhancement [39]–[42], gain enhancement [43], radiation pattern synthesis [44], [45], guiding the excitation position [46] and designing metasurface antennas [47]–[52]. The

This work is funded by China National Key Basic Research Program under Grant 2016YFA0301103, Shanghai Pujiang Program under Grant 20PJ1411400, and National Natural Science Foundation of China under Grant 91750102. (*Corresponding authors: Fang Guan and Feng Han Lin.*)

Jianping Zeng and Fang Guan are with the Institute for Nanoelectronic Devices and Quantum Computing and Zhangjiang Fudan International Innovation Center, Fudan University, Shanghai 200438, China, and Fang Guan is also with Peng Cheng Laboratory, Shengzhen 518000, China (e-mail: fguan@fudan.edu.cn).

Xiuye Liang and Jian Zi are with the State Key Laboratory of Surface Physics and the Department of Physics, Fudan University, Shanghai 200438, China.

Lianxing He is with the Institute of Satellite Electronics, Innovation Academy for Microsatellites of CAS, Shanghai 201210, China.

Feng Han Lin is with the School of Information Science and Technology, ShanghaiTech University, Shanghai 201210, China (linfh@shanghaitech.edu.cn).

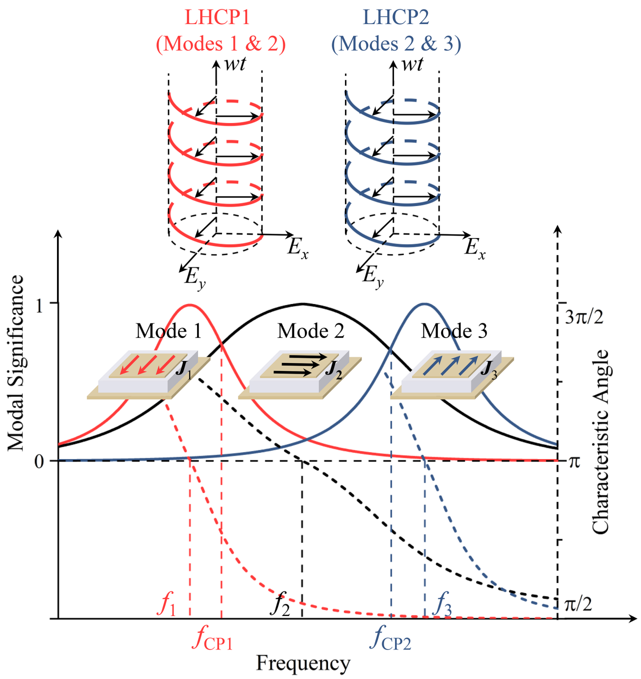

Fig. 1. Concept of triple-mode operation for wideband circular polarization. Mode 2 is wideband for being shared by modes 1 and 3. Modes 1 and 3 are of the same polarization but in opposite phase, and two resultant CP modes are of the same sense.

aforementioned applications of CMA are mostly focused on LP antennas due to the real nature of characteristic modes and the complex nature of CP modes, where the important inter-mode phase difference for CP radiation is less addressed [53]–[56].

In this paper, a method of triple-mode operation by *capacitive loading* is proposed for enhancing the CP bandwidth of single-fed microstrip patch antennas. Instead of using an even number of LP modes for multiple CP modes, an odd number of LP modes are leveraged by capacitive slot loading of microstrip patch antennas. CMA is utilized for revealing the operating mechanisms of the multi-mode CP antennas. With a single-fed, single-layer, and single-element structure, three orthogonal modes are simultaneously excited for improved CP bandwidth. For proof of concept, two popular slotted patch antennas are analyzed in detail, i.e., the U-slot and E-shaped patch antennas.

The paper is organized as follows. Section II briefly reviews the characteristic modes theory and illustrates the proposed triple-mode resonance design method. In Section III and Section IV, the U-slot and E-shaped wideband CP patch antennas are investigated, respectively. The CMA results, parametric study, empirical design formulas and design progress are presented in detail. Section V presents the experimental results and discussion, followed by conclusions in Section VI.

II. Design Method

The characteristic mode theory is briefly reviewed and used for analyzing the working principle of the proposed antennas, and expound the proposed triple-mode design method.

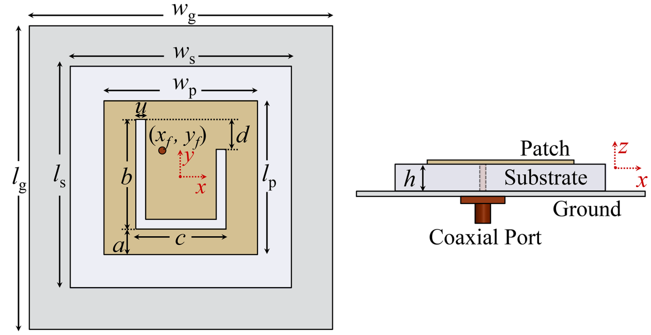

Fig. 2. Geometry of the proposed U-slot CP patch antenna. Dimensions are $w_g = l_g = 60$, $w_s = l_s = 25.2$, $w_p = l_p = 13.2$, $h = 6.3$, $a = 2.2$, $b = 9.4$, $c = 7.7$, $d = 2.6$, $u = 0.8$, $x_f = -1.6$, $y_f = 2.3$ (Unit: millimeter).

A. Characteristic Mode Theory

The total currents $\boldsymbol{J}$ on the perfect electric conductor (PEC) can be expressed as a linear superposition of the characteristic currents, defined as

$$\boldsymbol{J} = \sum_{n=1}^{N} c_n \boldsymbol{J}_n, \tag{1}$$

where $\boldsymbol{J}_n$ is the characteristic current of mode n. c_n is the complex modal weighting coefficient of the n-th order mode [36]–[38].

Two parameters are important for CP antenna design, namely the modal significance (MS) and the characteristic angle (CA), both as a function of the eigenvalue (λ_n), defined as

$$\mathrm{MS}_n = 1/|1 + j\lambda_n|, \tag{2}$$

$$\mathrm{CA}_n = \pi - \tan^{-1}(\lambda_n). \tag{3}$$

MS_n represents the potential contribution of a particular mode to the total radiation when a source or excitation is applied. CA_n physically characterizes the phase angle between a characteristic current and the corresponding characteristic far field. A mode is at resonance with MS equal to one or with CA_n close to π [36]–[38]. For CP radiation, at least two modes should be excited simultaneously with equal MS and 90-degree CA difference.

B. Concept: Triple-mode Wideband CP Operation

Fig. 1 shows the proposed key concept of triple-mode operation for wideband CP radiation. With three modes, 90-degree CA difference is desired for both the mode pair (1 and 2) and pair (2 and 3), where each pair of modes is orthogonally-polarized. Mode 2 of resonant frequency f_2 is a wideband mode shared by two relatively narrow-band modes, including the mode 1 resonant at f_1 and mode 3 resonant at f_3. $\boldsymbol{J}_1$ and $\boldsymbol{J}_3$ are of the same polarization but in opposite phase, which is further perpendicular to the polarization of $\boldsymbol{J}_2$. As a result, two CP modes are formed by ($\boldsymbol{J}_1$+$\boldsymbol{J}_2$) at a lower band and ($\boldsymbol{J}_2$+$\boldsymbol{J}_3$) at a higher band, respectively. From the characteristic angle curve, the phase of mode 1 lags behind that of mode 2, and the phase of mode 2 lags behind that of mode 3. Therefore, the two CP modes are of the same sense, leading to improved CP bandwidth. The concept is verified by two examples, a U-slot antenna and an E-shaped antenna. The operating modes of the former include a slot mode, a TM_{10}-like mode and a TM_{01}-like

This article has been accepted for publication in a future issue of this journal, but has not been fully edited. Content may change prior to final publication. Citation information: DOI 10.1109/TAP.2021.3111280, IEEE Transactions on Antennas and Propagation

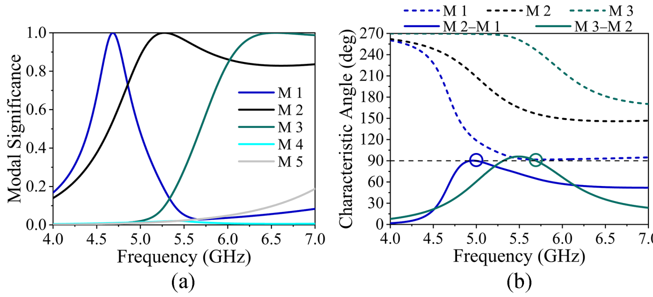

Fig. 3. (a) Modal significance and (b) Characteristic angle of U-slot structure. The characteristic angle difference between the Mode 2 and 1 is represented by M 2 – M 1, and the characteristic angle difference between the Mode 3 and 2 is represented by M 3 – M 2.

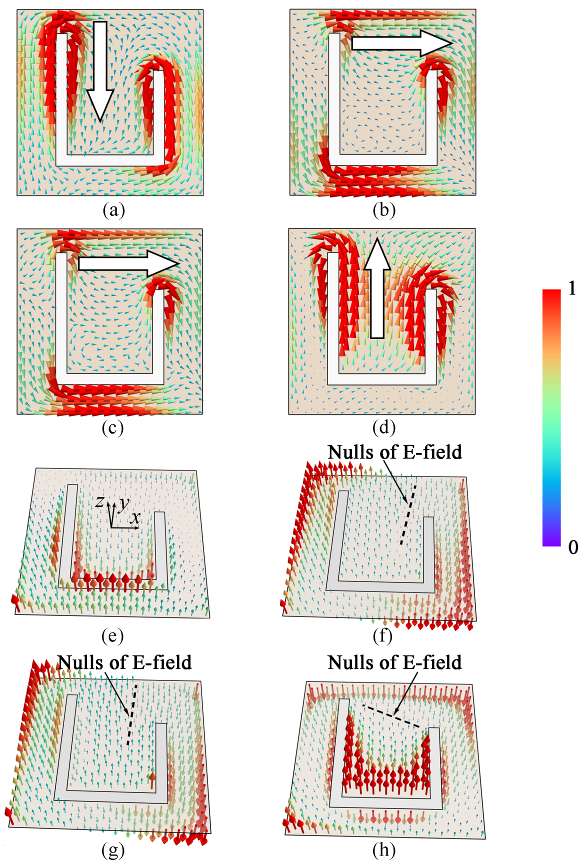

Fig. 4. Modal currents and electric fields of the U-slot structure. (a) $\boldsymbol{J}_1$ at 5.0 GHz. (b) $\boldsymbol{J}_2$ at 5.0 GHz. (c) $\boldsymbol{J}_2$ at 5.7 GHz. (d) $\boldsymbol{J}_3$ at 5.7 GHz. (e) $\boldsymbol{E}_1$ at 5.0 GHz. (f) $\boldsymbol{E}_2$ at 5.0 GHz. (g) $\boldsymbol{E}_2$ at 5.7 GHz. (h) $\boldsymbol{E}_3$ at 5.7 GHz. The main directions of the modal currents around the feeding position are also added to the figure in the form of bold white arrow. The modal currents and electric fields are normalized, and the color bar reflects their relative intensity.

mode; whereas a TM_{10}-like mode, a TM_{01}-like mode and a TM_{11}-like mode for the latter.

III. Wideband U-slot CP Patch Antenna

A. CMA of U-slot Structure

Fig. 2 shows the configuration of the U-slot CP antenna. The antenna is composed of a top metallic patch ($w_p \times l_p$), a dielectric substrate of Rogers AD250C ($w_s \times l_s$, $\varepsilon_r = 2.5$, $\tan\delta = 0.0013$ and thickness of 6.3 mm) and a ground plane ($w_g \times l_g$). Other structural parameters of the antenna are listed in the caption of Fig. 2. An asymmetric U-slot is cut on the top

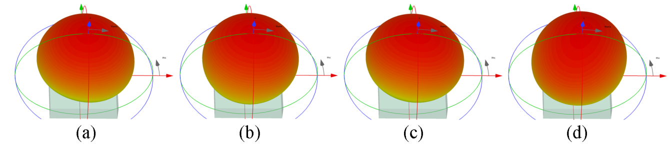

Fig. 5. Modal radiation patterns of the U-slot structure. (a) Mode 1 at 5.0 GHz. (b) Mode 2 at 5.0 GHz. (c) Mode 2 at 5.7 GHz. (d) Mode 3 at 5.7 GHz.

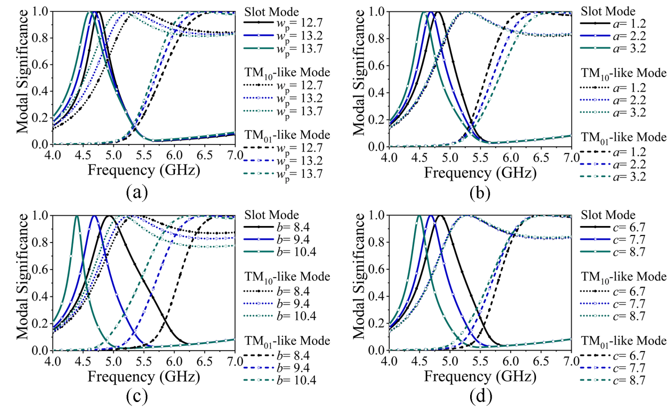

Fig. 6. Effects of different dimensions on modal significance of U-slot structure. (a) w_p. (b) a. (c) b. (d) c.

metallic patch, which introduces a new slot mode for CP operation and helps with the impedance matching. The probe feed position is offset from the y-axis.

Fig. 3 shows the CMA results of the first five modes for the U-slot structure, where the substrate and ground plane layers are infinite extended in the z-plane. As can be seen, two mode pairs (1 and 2) and (2 and 3) are formed, each pair with an intrinsically 90-degree phase difference and similar MS. Mode 1 is the slot mode resonant at approximately 4.7 GHz. For the first and second mode pairs, the 90-degree phase difference occurs at approximately 5.0 GHz and 5.7 GHz, respectively. In addition, as can be seen from Fig. 3(b), the phase of mode 1 lags behind mode 2, whereas that of mode 3 leads mode 2. The two pairs of modes can be excited for improving CP bandwidth according to the proposed concept.

Fig. 4 shows the associated modal currents and E-fields of the three modes at 5.0 GHz or 5.7 GHz where CA difference is equal to 90 degrees. As can be seen, the modal currents, electric fields, and modal radiation patterns of the same mode at different frequencies are similar. $\boldsymbol{J}_1$ and $\boldsymbol{J}_3$ are mainly vertically directed whereas $\boldsymbol{J}_2$ is mainly horizontally directed. Fig. 4(f)–(h) show that the nulls of E-field approximately extend along the y-axis for Mode 2 but along the x-axis for mode 3. The asymmetric U-slot disturbs the original electric field distribution and results in the offset of the nulls of the E-field from the central lines. The results are similar to those of the TM_{10} and TM_{01} modes of conventional square patch antennas. Therefore, the Modes 1–3 are named as the slot mode, the TM_{10}-like mode and the TM_{01}-like mode, respectively. Fig. 5 shows the modal radiation patterns of the three modes at 5.0 GHz or 5.7 GHz. All the three modes generate broadside radiation patterns.

To excite the three modes, a probe is placed close to the U-slot (as shown in Fig. 2), where the characteristic E-field of all the three modes are non-zero (as shown in Fig. 4). With the

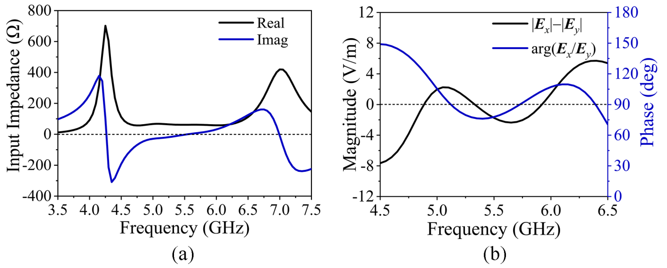

Fig. 7. (a) Input impedance of the U-slot CP patch antenna and (b) Magnitude and phase of $\boldsymbol{E}_x$ and $\boldsymbol{E}_y$ components of the U-slot CP patch antenna at the broadside direction.

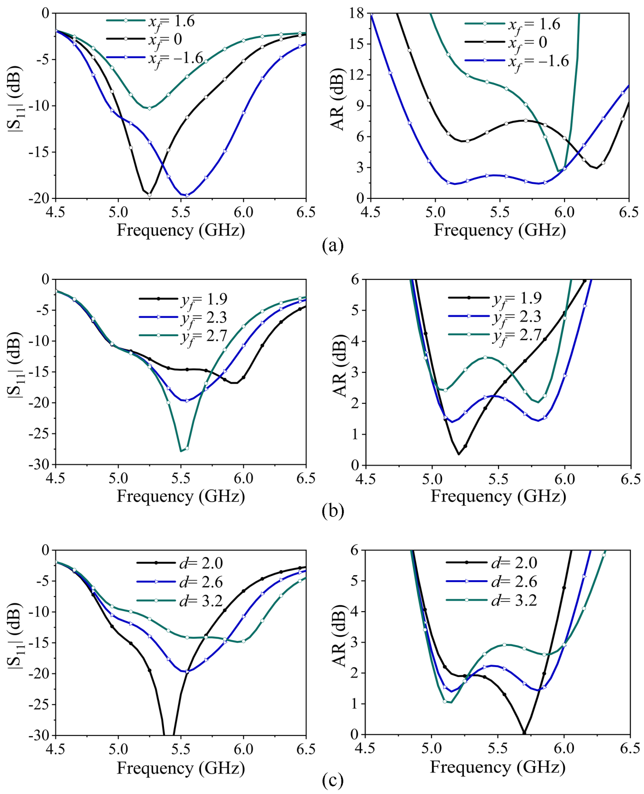

Fig. 8. Effects of different dimensions on $|S_{11}|$ and AR of the U-slot CP patch antenna. (a) x_f. (b) y_f. (c) d.

feeding area determined with the aid of CMA, the optimum feeding position is further optimized (in Section B).

B. Parametric Study

Key parameters are studied using CMA for understanding how the mode behavior is affected, followed by a quantitative optimization of the antenna performance.

Fig. 6 shows the effects of w_p, a, b, and c on the resonant frequencies and the modal significances. As can be seen from Fig. 6(a), the resonant frequencies of the $TM_{10/01}$-like modes both increase with smaller w_p owing to reduced electrical size of the resonator. The slot mode is almost unaffected. As shown in Figs. 6(b)–(d), the slot mode is mainly affected by its length and position. The resonant frequency of the TM_{01}-like mode changes with the U-slot geometry due to similar current distribution. By contrast, the TM_{10}-like mode is almost unaffected because of its horizontally directed current distribution. The variation of these three modes with the above parameters can also be analyzed in combination with their current distribution as shown in Fig. 4, and the results are consistent.

The parametric study with CMA provides insights for manipulating the mode distribution against frequency. With the coaxial probe included, the antenna is further quantitatively investigated for optimum performance.

Fig. 7(a) shows the input impedance of the optimum U-slot CP patch antenna. As can be seen, the input reactance across zero for three times, associated with the three modes aforementioned. The resonant frequencies are not strictly corresponded due to the reactive loading of the feeding probe. Fig. 7(b) shows the $\boldsymbol{E}_x$ and $\boldsymbol{E}_y$ components in far field along positive z axis. In the band of interest, the amplitude and phase both vary smoothly, implying a wide AR bandwidth. The differences of the amplitude and the phase both cross the critical line twice, indicating two AR minimum poles.

Fig. 8 shows the effects of the feeding position (x_f, y_f) and the length of U-slot (d) on the $|S_{11}|$ and AR. As can be observed from Fig. 8(a), when x_f increases (corresponding to a shift of the probe toward positive x-axis), both the impedance matching and AR become worse. As can be observed from Fig. 8(b), the impedance bandwidth reduces and AR increases with growing y_f. For smaller y_f, the impedance bandwidth is large but the AR bandwidth reduces. As can be seen from Fig. 8(c), the effect of decreasing d is similar to that of increasing y_f. In summary, the feeding position and the length of U-slot can be optimized for impedance matching and AR by adjusting x_f, y_f, and d.

C. Empirical Design Formulas

Empirical formulas are necessary for fast engineering design. Therefore, the empirical formulas for estimating the three modal resonant frequencies based on CMA are derived. The resonant frequencies correspond to half of the working wavelength, that is

$$f = c\Big/\left(2l_{eff}\sqrt{\varepsilon_{eff}}\right), \tag{4}$$

$$\varepsilon_{eff} = \frac{\varepsilon_r+1}{2} + \frac{\varepsilon_r-1}{2}\left(1+\frac{10h}{w_\mathrm{p}}\right)^{-1/2}, \tag{5}$$

where c is the speed of light in free space, ε_{eff} is the effective permittivity of substrate, and l_{eff} is the effective length.

The next is to find the effective length of the three modes. Since the current of the TM_{01}-like mode is interrupted by the horizontal slot, the formulas of its resonant frequency need to be revised. Based on the modal current distribution,

$$l_{eff}^{\mathrm{Slot}} = 2b - d + c - 2u, \tag{6}$$

$$l_{eff}^{\mathrm{TM_{10}\text{-like}}} = w_\mathrm{p} + 2\Delta l\left(l_\mathrm{p}\right), \tag{7}$$

$$l_{eff}^{\mathrm{TM_{01}\text{-like}}} = l_\mathrm{p} - a - u + 2\Delta l\left(w_\mathrm{p}\right), \tag{8}$$

$$\Delta l\left(l_\mathrm{p}\right) = 0.412h\left(\frac{\varepsilon_{eff}+0.3}{\varepsilon_{eff}-0.258}\right)\left(\frac{l_\mathrm{p}/h+0.264}{l_\mathrm{p}/h+0.8}\right), \tag{9}$$

$$\Delta l\left(w_\mathrm{p}\right) = 0.412h\left(\frac{\varepsilon_{eff}+0.3}{\varepsilon_{eff}-0.258}\right)\left(\frac{w_\mathrm{p}/h+0.264}{w_\mathrm{p}/h+0.8}\right), \tag{10}$$

where b, d, c, u, w_p, l_p, and a are structural parameters shown in the caption of Fig. 2. The terms $\Delta l(l_p)$ and $\Delta l(w_p)$ are the extended lengths of the two sides of the patch antenna due to

This article has been accepted for publication in a future issue of this journal, but has not been fully edited. Content may change prior to final publication. Citation information: DOI 10.1109/TAP.2021.3111280, IEEE Transactions on Antennas and Propagation

TABLE I
COMPARISONS BETWEEN EMPIRICAL FORMULAS AND CMA FOR U-SLOT CP ANTENNA

Resonant Frequency	f_{Slot}	$f_{TM10\text{-}like}$	$f_{TM01\text{-}like}$
Empirical Formulas	4.69 GHz	5.56 GHz	6.62 GHz
CMA	4.70 GHz	5.30 GHz	6.56 GHz

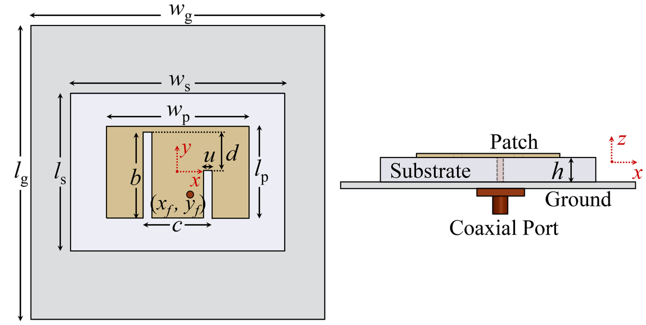

Fig. 9. Geometry of the proposed E-shaped CP patch antenna. Dimensions are $w_g = l_g = 60$, $w_s = 42.2$, $l_s = 24.2$, $w_p = 29.7$, $l_p = 12.8$, $h = 6.3$, $b = 12$, $c = 10$, $d = 5.3$, $u = 1.2$, $x_f = 1.7$, $y_f = -2.7$ (Unit: millimeter).

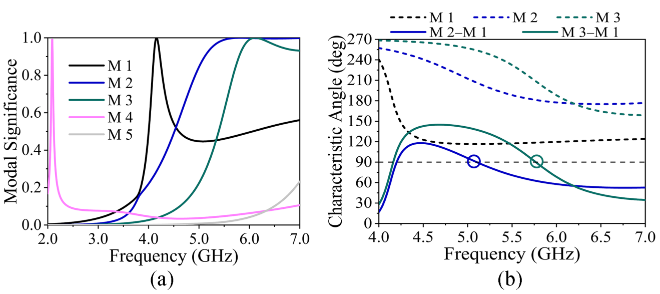

Fig. 10. (a) Modal significance and (b) Characteristic angle of the E-shaped structure. The characteristic angle difference between the Mode 2 and 1 is represented by M 2–M 1, and the characteristic angle difference between the Mode 3 and 1 is represented by M 3–M 1.

the edge effect, respectively [2].

Substituting (6)–(8) into (4), we can obtain the resonant frequencies of the three modes. The results obtained from empirical formulas and CMA are compared in Table I with good agreement. The empirical formulas are helpful for faster estimating the size of antennas.

The design process of U-slot antenna is summarized. Firstly, the characteristic modes of U-slot structure are analyzed to reveal the working principle of wideband circular polarization. Then, key parameters are qualitatively analyzed and quantitatively optimized. Finally, some empirical formulas are derived based on CMA.

IV. WIDEBAND E-SHAPED CP PATCH ANTENNA

The proposed method is further validated in the design of a E-shaped CP patch antenna. The configuration of the proposed E-shaped CP patch antenna is shown in Fig. 9. The dielectric substrate used is the same as that in the U-slot antenna design.

A. CMA of E-shaped Structure

The CMA's results of the optimum E-shaped CP patch antenna are shown in Fig. 10–12. As can be seen from Fig. 10, mode 4 resonates at about 2.1 GHz is the slot mode and cannot be effectively excited at the center frequency of 5.5 GHz.

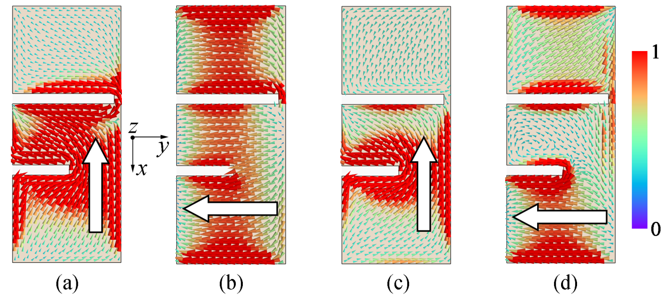

Fig. 11. Modal currents of the E-shaped CP structure. (a) $\boldsymbol{J}_1$ at 5.1 GHz (TM_{10}-like mode). (b) $\boldsymbol{J}_2$ at 5.1 GHz (TM_{01}-like mode). (c) $\boldsymbol{J}_1$ at 5.8 GHz (TM_{10}-like mode). (d) $\boldsymbol{J}_3$ at 5.8 GHz (TM_{11}-like mode). The main direction of the modal currents around the feeding position are also added to the figure in the form of bold white arrow. The modal currents and electric fields are normalized, and the color bar reflects their relative size intensity.

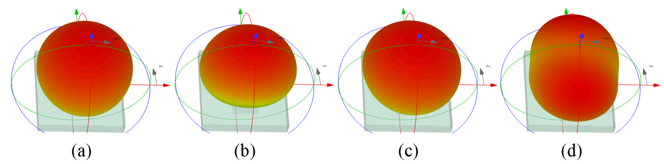

Fig. 12. Modal radiation patterns of the E-shaped structure. (a) Mode 1 at 5.1 GHz. (b) Mode 2 at 5.1 GHz. (c) Mode 1 at 5.8 GHz. (d) Mode 3 at 5.8 GHz.

Therefore, the three modes to be used include the TM_{10}-like mode (mode 1), the TM_{01}-like mode (mode 2), and the TM_{11}-like mode (mode 3). Two pair of modes are formed (mode pair 1 & 2 and mode pair 1 & 3), each pair with 90-degree phase difference and similar MS. For the first pair, mode 1 and mode 2 exhibit a 90-degree phase difference at about 5.1 GHz. For the second pair, mode 1 and mode 3 also exhibit a 90-degree phase difference but at a higher frequency of approximately 5.8 GHz. It means that two AR minima poles will be formed to realize wideband circular polarization.

Fig. 11 shows the modal currents of the three modes at 5.1 GHz or 5.8 GHz where CA difference is equal to 90 degrees. As can be seen, the modal currents and modal radiation patterns of the same mode at different frequencies are similar. $\boldsymbol{J}_1$ is mainly in the x direction, $\boldsymbol{J}_2$ and $\boldsymbol{J}_3$ are mainly in the y direction. Although the slot mode does not directly participate in the radiation, the slot plays a key role in manipulating the TM_{10}-like mode. The long vertical slot arm has an obvious blocking effect on the horizontal current, and the current path of TM_{10}-like mode starts from the patch's edge and ends at the long vertical slot arm. In addition, all the three modes almost generate broadside radiation patterns, as shown in Fig. 12.

In short, the triple-mode design method to realize wideband circular polarization is consistent with that of the proposed U-slot structure above, but the three modes used are not exactly the same.

The feeding scheme follows the principles from the U-slot design. As shown in Fig. 9, the probe is placed near the inner edge of the shorter vertical slot arm. With the approximate feeding area determined, the optimum feeding position is further optimized through parametric analysis (in section B).

B. Parametric Study

With the coaxial probe included, the antenna is further quantitatively investigated for optimum performance.

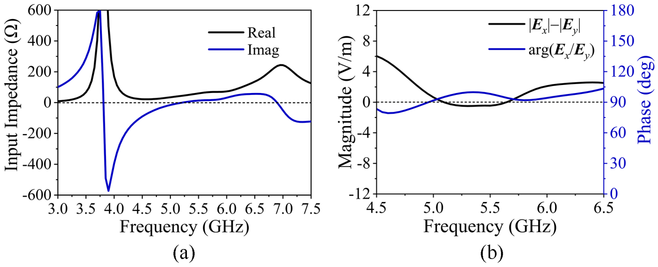

Fig. 13. (a) Input impedance of the E-shaped CP patch antenna and (b) Magnitude and phase of $\boldsymbol{E}_x$ and $\boldsymbol{E}_y$ components of the E-shaped CP patch antenna at the broadside direction.

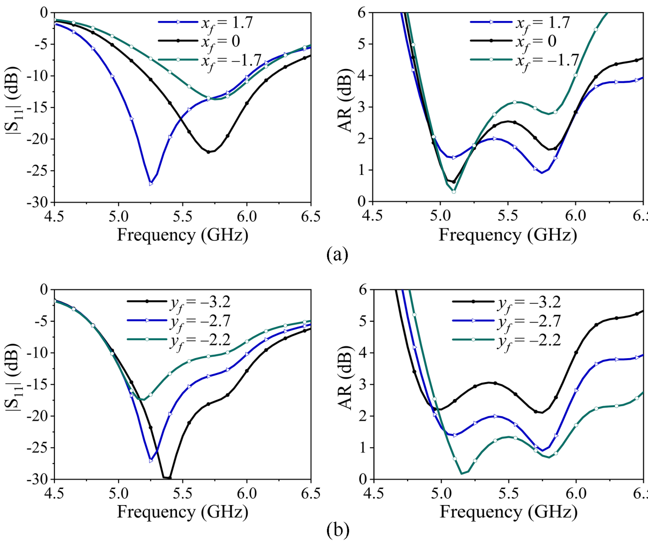

Fig. 14. Effects of different dimensions on $|S_{11}|$ and AR of the E-shaped CP patch antenna. (a) x_f. (b) y_f.

Fig. 13(a) shows the input impedance of the optimum E-shaped CP patch antenna. Similar to the proposed U-slot CP antenna, the input reactance crosses zero for three times. In the band of interest, both the input resistance and reactance vary smoothly against frequency, a result of combined triple-mode contribution. Fig. 13(b) shows the $\boldsymbol{E}_x$ and $\boldsymbol{E}_y$ components in far field along positive z axis. The amplitude and phase differences of far-field $\boldsymbol{E}_x$ and $\boldsymbol{E}_y$ components along z-propagation varies around 0 V and 90 degrees, respectively. The amplitude and phase differences of the two components have crossed the critical line twice, indicating a wideband AR performance of two AR minima poles. The results are consistent with those from CMA.

Fig. 14 shows the effects of different feeding position on $|S_{11}|$ and AR for the E-shaped CP patch antenna. As can be seen from Fig. 14(a) and 14(b), decreasing x_f does not provide good impedance matching and AR whilst y_f can be optimized for a tradeoff between the impedance and AR bandwidth.

Based on the two cases of U-slot antenna and E-shaped antenna, it can be safely concluded that the optimum feeding area guided by CMA is helpful for estimating the optimum feeding position. In addition, the feeding position is the key to exciting the three desired modes simultaneously for wideband circular radiation.

TABLE II
COMPARISONS BETWEEN EMPIRICAL FORMULAS AND CMA FOR E-SHAPED CP ANTENNA

Resonant Frequency	$f_{\text{TM10-like}}$	$f_{\text{TM01-like}}$	$f_{\text{TM11-like}}$
Empirical Formulas	4.32 GHz	5.39 GHz	6.11 GHz
CMA	4.28 GHz	5.77 GHz	6.16 GHz

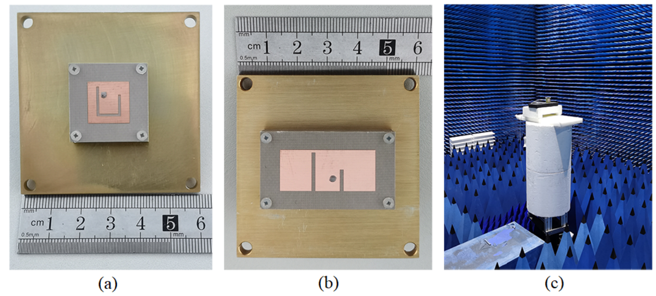

Fig. 15. Photograph of (a) the fabricated U-slot CP patch antenna. (b) the fabricated E-shaped CP patch antenna. (c) Far-field measurement environment.

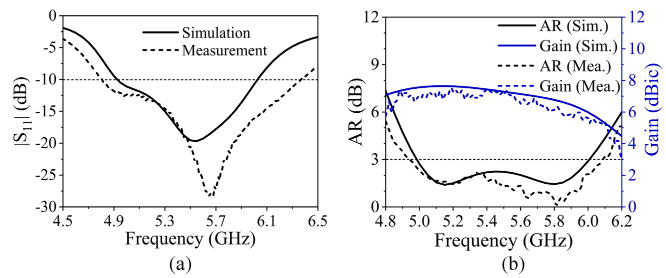

Fig. 16. Simulated and measured results of the U-slot CP patch antenna. (a) $|S_{11}|$. (b) AR and boresight gain.

C. *Empirical Design Formulas*

Since the current of the TM_{10}-like mode is interrupted by the longer vertical slot, the formulas of its resonant frequency are revised. Based on the modal current distribution,

$$l_{eff}^{\text{TM}_{10}\text{-like}} = w_p/2 + c/2 - u + 2\Delta l\left(l_p\right), \tag{11}$$

$$l_{eff}^{\text{TM}_{01}\text{-like}} = l_p + 2\Delta l\left(w_p\right), \tag{12}$$

$$l_{eff}^{\text{TM}_{11}\text{-like}} = \left[\left(\frac{1}{w_p + 2\Delta l\left(l_p\right)}\right)^2 + \left(\frac{1}{l_p + 2\Delta l\left(w_p\right)}\right)^2\right]^{-1/2}, \tag{13}$$

where w_p, c, u, l_p, and w_p are structural parameters shown in the caption of Fig. 10. The terms $\Delta l(w_p)$ and $\Delta l(l_p)$ are the extended lengths due to the edge effect [2].

Substituting (11)–(13) into (4), the resonant frequencies are calculated. Table II shows the comparisons of resonant frequencies calculated by CMA and by the empirical formulas with good agreement.

The design process for the E-shaped CP patch antenna is similar to that of the U-slot antenna. For brevity, we do not repeat it again.

V. EXPERIMENTAL RESULTS AND DISCUSSION

To validate the analysis and design of the two proposed antennas, prototypes of U-slot and E-shaped CP patch antennas are fabricated and measured, as shown in Fig. 15–19. The

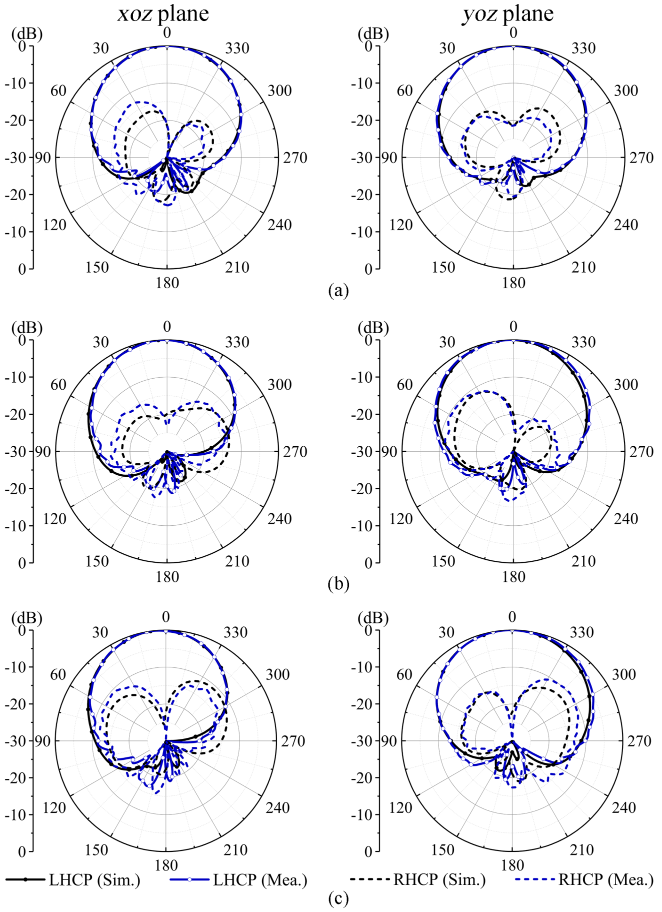

Fig. 17. Simulated and measured normalized radiation patterns of the U-slot CP patch antenna. (a) 5.2 GHz. (b) 5.5 GHz. (c) 5.8 GHz.

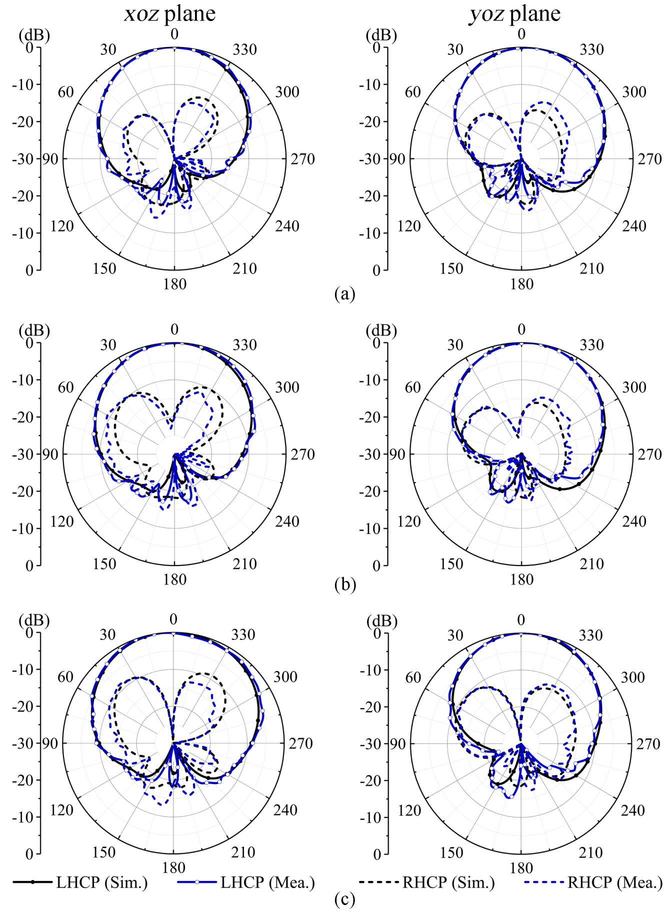

Fig. 19. Simulated and measured normalized radiation patterns of the E-shaped CP patch antenna. (a) 5.2 GHz. (b) 5.5 GHz. (c) 5.8 GHz.

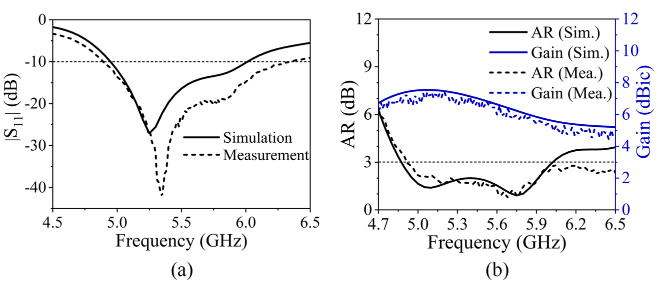

Fg. 18. Simulated and measured results of the E-shaped CP patch antenna. (a) $|S_{11}|$. (b) AR and boresight gain.

simulated and measured $|S_{11}|$, gain, AR, and radiation patterns are in good agreement. For the U-slot / E-shaped patch antenna, the measured 10-dB impedance bandwidth and the 3-dB AR bandwidth are 4.80–6.37 GHz / 4.89–6.34 GHz and 4.93–6.09 GHz / 4.91–6.50 GHz, respectively. The overlapping bandwidth are 21.1% (4.93–6.09 GHz) and 25.4% (4.91–6.34 GHz), respectively. The boresight gain varies from 5.2 to 7.4 dBic (for U-slot) and 5.0 to 7.3 dBic (for E-shaped) in the overlapping bandwidth, respectively. For both antennas, three modes are excited with two AR minima poles present in operating band, which is the key to increase the CP bandwidth without greatly increasing the antenna volume.

The simulated and measured radiation patterns are shown in Fig. 17 and 19. The beam squint is mainly caused by the off-center feeding probe and asymmetric slots. These two factors make the amplitude and phase distribution of surface current asymmetric and result in the beam squint. Moreover, the beam squint is more obvious in the high frequency band, resulting in the decrease of the boresight gain in the high frequency band. The phenomenon of similar structures also appears in references [16], [23], [27]. The cross-polarization level is better than –15 dB at the broadside direction across the bandwidth.

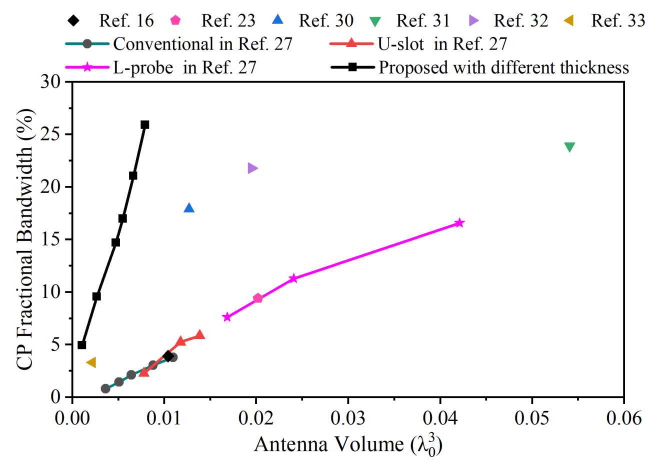

Fig. 20. Comparisons of the CP fractional bandwidth and antenna volume for the proposed U-slot antennas and other kinds of CP patch antennas. (λ_0: Corresponding to the center operation frequency, and the CP fractional bandwidth is defined as the bandwidth overlapped by 10-dB return loss and 3-dB AR)

TABLE III
COMPARISONS OF DIFFERENT WIDEBAND CP PATCH ANTENNAS

Refs	Dimension (λ_0^3)	Overlapping Bandwidth	Peak Gain (dBic)	AR Poles	Number of Layers	Number of Elements	Approaches
[9]	1.66*1.66*0.058	5.2	10.5	2	2	4	Multi-feed Network
[10]	1.82*1.82*0.036	12.5	12	2	1	4	Multi-feed Network
[31]	0.64*0.64*0.132	23.9	8.7	2	1	5	Parasitic elements, thick air substrate,
[33]	0.51*0.27*0.016	3.3	2.7	2	1	3	Parasitic elements
[32]	0.59*0.59*0.056	21.8	7.6	2	2	17	Stacked patches, metasurface
[30]	0.38*0.38*0.088	17.9	8.8	2	2	2	Stacked patches, L-shaped strip feeding
[27]	0.42*0.42*0.221	11.8	NG	1	1	1	Thick air substrate, L-probe, truncating corners
[16]	0.35*0.35*0.085	3.9	8	1	1	1	Thick air substrate, unequal-arms U-slot
[23]	0.62*0.37*0.088	9.4	8.3	1	1	1	Thick air substrate, unequal-arms E-shaped
[27]	0.38*0.38*0.050	2.2	NG	1	1	1	Thick air substrate, U-slot, truncating corners
[27]	0.37*0.37*0.100	4.3	NG	1	1	1	Thick air substrate, U-slot, truncating corners
This work (U-slot)	0.24*0.24*0.115	21.1	7.4	2	1	1	Triple modes: Slot, TM_{10}-like, TM_{01}-like
This work (E-shaped)	0.55*0.23*0.114	25.4	7.3	2	1	1	Triple modes: TM_{10}-like, TM_{01}-like, TM_{11}-like

λ_0: Corresponding to the center operation frequency
Overlapping Bandwidth: The bandwidth overlapped by 10-dB return loss and 3-dB AR
NG: Not given in the corresponding references

To highlight the novelties and advantages of the two proposed antennas, the comparison results with reported works are shown in Fig. 20 and the details are listed in Table III. For fair comparison, the proposed U-slot CP patch antenna is optimized at different dielectric thicknesses based on the proposed triple-mode operation, including h = 2, 3, 4, 5, 6.3, and 8 mm. The center frequencies of CP U-slot antennas with different dielectric thicknesses are all optimized to about 5.5 GHz. As can be seen, the proposed CP antennas have the advantages of simpler structure, smaller size, and larger bandwidth. For example, the CP bandwidths of the proposed two antennas both excess 21.1%, which are about 4.9 times wider than the conventional corner-truncated U-slot patch antennas (4.3% in bandwidth) under the similar thickness, and 9.4 times wider than the conventional corner-truncated U-slot patch (2.2% in bandwidth) under the similar volume [27].

VI. CONCLUSION

A method of triple-mode operation by capacitive loading is proposed for significant bandwidth enhancement of single-feed CP microstrip patch antennas with the aid of CMA. Guided by the proposed method, two types of triple-mode CP antennas are thoroughly analyzed and experimentally verified for proof of concept. The proposed U-slot antenna works with the slot mode, TM_{10}-like mode, and TM_{01}-like mode and the proposed E-shaped antenna works with the TM_{10}-like mode, TM_{01}-like mode, and TM_{11}-like mode. Two important functions of resonant-slot loading are revealed with CMA, including the introduction of additional modes and the manipulation of microstrip patch modes. In addition to the revealed new physical insights and performance improvements, the application of CMA in antenna engineering is further extended to the derivation of mode-based empirical formulas for fast engineering design. The proposed antenna designs can be good candidates for CP phased array in space applications. Since the proposed triple-mode CP concept is independent of any specific structure, the method can be extended to other types of CP antennas, making a timely contribution to the development of the next generation of space-ground-integrated smart networks.

REFERENCES

[1] S. Gao, Q. Luo, and F. Zhu, *Circularly Polarized Antennas*. Hoboken, NJ, USA: Wiley-IEEE Press, Nov. 2013.
[2] C. A. Balanis, *Antenna Theory Analysis and Design*. 3rd ed. Hoboken, NJ, USA: Wiley, 2005.
[3] D. M. Pozar, “Microstrip antennas,” *Proc. IEEE*, vol. 80, no. 1, pp. 70–91,1992.
[4] K. F. Lee and K. F. Tong, “Microstrip patch antennas-basic characteristics and some recent advances”, *Proc. IEEE*, vol. 100, no. 7, pp. 2169-2180, Jul. 2012.
[5] J. R. James, P. S. Hall, and C. Wood, *Microstrip Antenna Theory and Design*. Stevenage, U.K.: Peter Peregrinus, 1981.
[6] P. Sharma and K. Gupta, “Analysis and optimized design of single feed circularly polarized microstrip antennas,” *IEEE Trans. Antennas Propag.,* vol. AP-31, no. 6, pp. 949–955, Nov. 1983.
[7] Nasimuddin, Z. N. Chen, and X. M. Qing, “A compact circularly polarized cross-shaped slotted microstrip antenna,” *IEEE Trans. Antennas Propag.*, vol. 60, no. 3, pp. 1584–1588, Mar. 2012.
[8] S. C. Chen, G. C. Liu, X. Y. Chen, T. F. Lin, X. G. Liu, and Z. Q. Duan, “Compact dual-band GPS microstrip antenna using multilayer LTCC Substrate,” *IEEE Antennas Wireless Propag. Lett.*, vol. 9, pp. 421–423, 2010.
[9] Y. Li, Z. Zhang, and Z. Feng, “A sequential-phase feed using a circularly polarized shorted loop structure,” *IEEE Trans. Antennas Propag.*, vol. 61, no. 3, pp. 1443–1447, March 2013.
[10] C. Deng, Y. Li, Z. Zhang, and Z. Feng, “A wideband sequential-phase fed circularly polarized patch array,” *IEEE Trans. Antennas Propag.*, vol. 62, no. 7, pp. 3890–3893, Jul. 2014.
[11] J. Kovitz and Y. Rahmat-Samii, “Using thick substrate and capacitive probe compensation to enhance the bandwidth of traditional CP patch antennas,” *IEEE Trans. Antennas Propag.*, vol. 62, no. 10, pp. 4970–4979, Oct. 2014.
[12] Q. W. Lin, H. Wong, X. Y. Zhang, and H. W. Lai, “Printed meandering probe-fed circularly polarized patch antenna with wide bandwidth,” *IEEE Antennas Wireless Propag. Lett.*, vol. 13, pp. 654–657, 2014.
[13] B. P. Kumar, D. Guha, and C. Kumar, “Reduction of beam squinting and cross-polarized fields in a wideband CP element,” *IEEE Antennas Wireless Propag. Lett.*, vol. 19, no. 3, pp. 418–422, March 2020.
[14] M. Chen, W. Lu, L. Wang, M. Yang, and L. Zhu, “Design approach to a novel planar bisensing circularly polarized antenna,” *IEEE Trans. Antennas Propag.*, vol. 67, no. 11, pp. 6839–6846, Nov. 2019.
[15] T. Huynh and K. F. Lee, “Single-layer single-patch wideband microstrip antenna,” *Electron. Lett.,* vol. 31, no. 16, pp. 1310–1312, Aug. 1995.
[16] K. F. Tong and T. P. Wong, “Circularly polarized U-slot antenna,” *IEEE Trans. Antennas Propag.*, vol. 55, no. 8, pp. 2382–2385, Aug. 2007.

[17] W. Yin, X. Liang, A. Chen, Z. Zhang, L. Shi, F. Guan, X. Liu, and J. Zi, "Cross-polarization suppression for patch array antennas via generalized Kerker effects," *Opt. Express*, vol. 28, no. 1, pp. 40–47, Jan. 2020.

[18] K. F. Lee, S. L. S. Yang, A. A. Kishk, and K. M. Luk, "The vers1atile U-slot patch antenna," *IEEE Antennas Propag. Mag*., vol. 52, no. 1, pp. 71–88, Feb. 2010.

[19] K. Y. Lam, K.-M. Luk, K. F. Lee, H. Wong, and K. B. Ng, "Small circularly polarized U-slot wideband patch antenna," *IEEE Antennas Wireless Propag. Lett.*, vol. 10, pp. 87–90, 2011.

[20] T. H. Jang, H. Y. Kim, D. M. Kang, S. H. Kim, and C. S. Park, "60 GHz Low-Profile, Wideband dual-polarized U-Slot coupled patch antenna with high isolation," *IEEE Trans. Antennas Propag.*, vol. 67, no. 7, pp. 4453–4462, July 2019.

[21] S. Hasibi-Taheri, M. Rafaei-Booket, and A. Ghorbani, "Design and fabrication of an efficient metallic phased array for TACAN application," *IEEE Trans. Antennas Propag.*, vol. 68, no. 6, pp. 4979–4984, June 2020.

[22] F. Yang, X.-X. Zhang, X. Ye, and Y. Rahmat-Samii, "Wide-band E-shaped patch antennas for wireless communications," *IEEE Trans. Antennas Propag.*, vol. 49, no. 7, pp. 1094–1100, July 2001.

[23] A. Khidre, K. F. Lee, F. Yang, and A. Elsherbeni, "Wideband circularly polarized E-shaped patch antenna for wireless applications," *IEEE Antennas Propag. Mag*., vol. 52, no. 5, pp. 219–229, Oct. 2010.

[24] A. Khidre, K. F. Lee, F. Yang, and A. Z. Elsherbeni, "Circular polarization reconfigurable wideband E-shaped patch antenna for wireless applications," *IEEE Trans. Antennas Propag.*, vol. 61, no. 2, pp. 960–964, Feb. 2013.

[25] J. Yin, Q. Wu, C. Yu, H. Wang, and W. Hong, "Broadband symmetrical E-Shaped patch antenna with multimode resonance for 5G millimeter-wave applications," *IEEE Trans. Antennas Propag.*, vol. 67, no. 7, pp. 4474–4483, July 2019.

[26] Y. X. Guo, C. L. Mak, K. M. Luk, and K. F. Lee, "Analysis and design of L-probe proximity fed-patch antennas," *IEEE Trans. Antennas Propag.*, vol. 49, pp. 145–149, Feb. 2001.

[27] S. S. Yang, K.-F. Lee, and A. A. Kishk, "Design and study of wideband single feed circularly polarized microstrip antennas," *Prog. Electromagn. Res*., vol. 80, pp. 45–61, 2008.

[28] L. Qiu, L. Zhu, and Y. Xu, "Wideband low-profile circularly polarized patch antenna using 90° modified Schiffman phase shifter and meandering microstrip feed," *IEEE Trans. Antennas Propag.*, vol. 68, no. 7, pp. 5680–5685, July 2020.

[29] J. Sun and K. Luk, "A circularly polarized water patch antenna," *IEEE Antennas Wireless Propag. Lett.*, vol. 19, no. 6, pp. 926–929, June 2020.

[30] J. Wu, X. Ren, Z. Wang and Y. Yin, "Broadband circularly polarized antenna with L-shaped strip feeding and shorting-pin loading," *IEEE Antennas Wireless Propag. Lett.*, vol. 13, pp. 1733-1736, 2014.

[31] J. Wu, Y. Yin, Z. Wang, and R. Lian, "Broadband circularly polarized patch antenna with parasitic strips," *IEEE Antennas Wireless Propag. Lett.*, vol. 14, pp. 559–562, 2015.

[32] S. X. Ta and I. Park, "Low-profile broadband circularly polarized patch antenna using metasurface," *IEEE Trans. Antennas Propag.*, vol. 63, no. 12, pp. 5929–5934, Dec. 2015.

[33] J. Lin and Q. Chu, "Enhancing bandwidth of cp microstrip antenna by using parasitic patches in annular sector shapes to control electric field components," *IEEE Antennas Wireless Propag. Lett.*, vol. 17, no. 5, pp. 924–927, May 2018.

[34] M. SalarRahimi, V. Volski, and G. A. E. Vandenbosch, "Mutual coupling-based compact wideband circularly polarized antenna," *IEEE Trans. Antennas Propag.*, vol. 67, no. 7, pp. 4872–4877, Jul. 2019.

[35] N. Liu, L. Zhu, Z. Liu, G. Fu, and Y. Liu, "Design approach of a single circularly polarized patch antenna with enhanced AR-bandwidth under triple-mode resonance," *IEEE Trans. Antennas Propag.*, vol. 68, no. 8, pp. 5827–5834, Aug. 2020.

[36] Y. Chen and C. F. Wang, *Characteristic Modes: Theory and Applications in Antenna Engineering*. Hoboken, NJ, USA: Wiley, 2015.

[37] R. J. Garbacz, "Modal expansions for resonance scattering phenomena," *Proc. IEEE*, vol. 53, no. 8, pp. 856–864, Aug. 1965.

[38] R. F. Harrington and J. R. Mautz, "Theory of characteristic modes for conducting bodies," *IEEE Trans. Antennas Propag.*, vol. 19, no. 5, pp. 622–628, Sep. 1971.

[39] E. Antonino-Daviu, M. Fabres, M. Ferrando-Bataller, and V. M. R. Penarrocha, "Modal analysis and design of band-notched uwb planar monopole antennas," *IEEE Trans. Antennas Propag.*, vol. 58, no. 5, pp. 1457–1467, May 2010.

[40] M. Khan and D. Chatterjee, "Characteristic mode analysis of a class of empirical design techniques for probe-fed, U-Slot microstrip patch antennas," *IEEE Trans. Antennas Propag.*, vol. 64, no. 7, pp. 2758–2770, July 2016.

[41] M. Khan and D. Chatterjee, "Analysis of reactive loading in a u-slot microstrip patch using the theory of characteristic modes," *IEEE Antennas Propag. Mag*., vol. 60, no. 6, pp. 88–97, Dec. 2018.

[42] J. Lin and Q. Chu, "Increasing bandwidth of slot antennas with combined characteristic modes," *IEEE Trans. Antennas Propag.*, vol. 66, no. 6, pp. 3148–3153, June 2018.

[43] J. Lin and Q. Chu, "Enhancing gain of ring slot antennas with shorting strips," *IEEE Trans. Antennas Propag.*, vol. 67, no. 7, pp. 4397–4405, July 2019.

[44] Z. Liang, J. Ouyang, F. Yang, and L. Zhou, "Design of license plate rfid tag antenna using characteristic mode pattern synthesis," *IEEE Trans. Antennas Propag.*, vol. 65, no. 10, pp. 4964–4970, Oct. 2017.

[45] H. Li, S. Sun, W. Li, M. Wu, and C. Zhou, "Systematic pattern synthesis for single antennas using characteristic mode analysis," *IEEE Trans. Antennas Propag.*, vol. 68, no. 7, pp. 5199–5208, July 2020.

[46] E. Antonino-Daviu, M. Cabedo-Fabrés, M. Sonkki, N. Mohamed Mohamed-Hicho, and M. Ferrando-Bataller, "Design guidelines for the excitation of characteristic modes in slotted planar structures," *IEEE Trans. Antennas Propag.*, vol. 64, no. 12, pp. 5020–5029, Dec. 2016.

[47] F. H. Lin and Z. N. Chen, "Low-profile wideband metasurface antennas using characteristic mode analysis," *IEEE Trans. Antennas Propag.*, vol. 65, no. 4, pp. 1706–1713, April 2017.

[48] T. Li, and Z. N. Chen, "Metasurface-based shared-aperture 5G S/K band antenna using characteristic mode analysis," *IEEE Trans. Antennas Propag.,* vol. 66, no. 12, pp. 6742–6750, Dec. 2018.

[49] F. H. Lin, and Z. N. Chen, "A method of suppressing higher order modes for improving radiation performance of metasurface multiport antennas using characteristic mode analysis," *IEEE Trans. Antennas Propag.,* vol. 66, no. 4, pp. 1894–1902, Apr. 2018.

[50] F. H. Lin, and Z. N. Chen, "Truncated impedance sheet model for low-profile broadband nonresonant-cell metasurface antennas using characteristic mode analysis," *IEEE Trans. Antennas Propag*., vol. 66, no. 10, pp. 5043–5051, Oct. 2018.

[51] T. Li and Z. N. Chen, "Shared-surface dual-band antenna for 5G applications," *IEEE Trans. Antennas Propag.*, vol. 68, no. 2, pp. 1128–1133, Feb. 2020.

[52] N. Nie, X. Yang, Z. N. Chen, and B. Wang, "A low-profile wideband hybrid metasurface antenna array for 5G and WiFi systems," *IEEE Trans. Antennas Propag.*, vol. 68, no. 2, pp. 665–671, Feb. 2020.

[53] Y. Chen and C. Wang, "Characteristic-mode-based improvement of circularly polarized U-Slot and E-Shaped Patch Antennas," *IEEE Antennas Wireless Propag. Lett.*, vol. 11, pp. 1474–1477, 2012.

[54] Huy Hung Tran, Nghia Nguyen-Trong, and Amin M. Abbosh, "Simple design procedure of a broadband circularly polarized slot monopole antenna assisted by characteristic mode analysis," *IEEE Access*, vol. 6, pp. 78386–78393, Dec. 2018.

[55] R. Xu *et al*., "Analysis and design of ultrawideband circularly polarized antenna and array," *IEEE Trans. Antennas Propag.*, vol. 68, no. 12, pp. 7842–7853, Dec. 2020.

[56] C. Zhao and C. Wang, "Characteristic mode design of wide band circularly polarized patch antenna consisting of H-shaped unit cells," *IEEE Access*, vol. 6, pp. 25292–25299, 2018.

Jianping Zeng (S'20) was born in Ruijin, Jiangxi, China. He received the B.S. degree in applied physics from Jiangxi Normal University, in 2018. He is currently pursuing the Ph.D. degree with Fudan University, Shanghai, China.

His current research interests include antennas, RF/microwave circuits, applied electromagnetic theory, and articial bandgap materials.

Xiuye Liang (S'19) was born in Handan, Hebei, China, in 1993. He received the B.S. degree in optoelectronic information science and engineering from Jiangnan

This article has been accepted for publication in a future issue of this journal, but has not been fully edited. Content may change prior to final publication. Citation information: DOI 10.1109/TAP.2021.3111280, IEEE Transactions on Antennas and Propagation

University, Wuxi, China, in 2016. He is currently pursuing the Ph.D. degree with Fudan University, Shanghai, China.

His current research interests include phased array feed antennas, UWB antenna arrays, articial bandgap materials, and articial intelligence in antenna design.

Lianxing He was born in Lianyun, China. He received the M.S. and Ph.D. degrees from the Shanghai Institute of Ceramics, Chinese Academy of Sciences (CAS), in 1997 and 2000, respectively. He is currently working as a Research Fellow with the Innovation Academy for Microsatellites of CAS. He is also an Adjunct Professor with ShanghaiTech University.

His research interests include phased array antenna, space-borne antenna, novel antenna-based on EBG/PBG, and/or metamaterials.

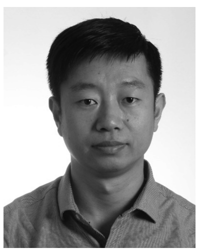

Fang Guan was born in Yixian, Liaoning, China, in 1979. He received the B.S. degree in applied physics from Fudan University, China, in 2002, and the M.S. and Ph.D. degrees in condensed matter physics from Fudan University, in 2005 and 2014, respectively. From 2014 to 2019, he was a Research Assistant with the Physics Department, Fudan University. He is currently an Associate Professor with the Institute for Nanoelectronic Devices and Quantum Computing, Fudan University.

His research interests include Photonic crystals, metasurfaces, phased arrays, and ultrawideband antenna arrays.

Feng Han Lin (S'12–SM'19) received the B. Eng and M. Eng degrees both in electrical engineering from Xidian University, Xi'an, China, in 2011 and 2014, respectively. He received the Ph.D. degree from the Department of Electrical and Computer Engineering, National University of Singapore (NUS), Singapore, in 2019. Since 2020, he has been with the School of Information Science and Technology, ShanghaiTech University, Shanghai, China, where he is currently an Assistant Professor.

His current research interests include applied electromagnetic theory, antennas and RF/microwave circuits.

Jian Zi was born in Sichuan, China. He received the B.S., M.S., and Ph.D. degrees from Fudan University, in 1985, 1988, and 1991, respectively. From 1991 to 1995, he was a Lecturer with the Department of Physics, Fudan University, and held the postdoctoral position with the University of Munster, Germany. From 1994 to 1995, he was an Associate Professor with the Department of Physics, Fudan University. Since 1996, he has been a Professor with the Department of Physics, Fudan University, and access to the National Science Fund for Distinguished Young ScholarsSince 2001, He has been a Chang-Jiang Professor nominated by the Ministry of Education of China. He was appointed as the Chief Scientist of the Project 973 by the Ministry of Science and Technology, in 2001 and 2007. He has authored or coauthored more than 300 technical articles.

His current research interests include photonic crystals, plasmonics, metamaterials, natural photonic structures and structural colors, and liquid surface waves propagating in periodic structures.